


Communication

Error Characterization of Differential Detection and Non-Differential Detection for MIMO UWOC Systems in Seawater Turbulent Channels

Tong Wang ^{1,2} , Xiaonan Yu ^{1,2,*}, Baiqiu Zhao ¹ and Diyue Pang ¹

¹ School of Photoelectric Engineering, Changchun University of Science and Technology, Changchun 130022, China; wangtong@cust.edu.cn (T.W.); 2022200060@mails.cust.edu.cn (B.Z.); dy.pang@mails.cust.edu.cn (D.P.)

² Key Laboratory of Photoelectric Measurement and Control and Optical Information Transfer Technology of Ministry of Education, Changchun University of Science and Technology, Changchun 130022, China

* Correspondence: yuxiaonan@cust.edu.cn

Abstract: Ocean turbulence is an important factor affecting the development of underwater wireless optical communication (UWOC). To improve the error characteristics of the underwater optical communication system, we propose a differential detection-based multi-receiver-multi-transmitter (MIMO) underwater laser communication transmission method. Additionally, we derive the expressions for calculating the average BER of the MIMO underwater wireless optical communication system with differential detection and non-differential detection in the case that the two transmitted beams are completely uncorrelated. The error characteristics of the MIMO system are simulated and analyzed from the perspective of ocean turbulence intensity and link distance. The simulation results show that the differential detection method has a lower average BER compared to the non-differential detection method in the case of moderate-to-strong ocean turbulence. In addition, the differential detection methods do not have the error floor effect, and non-differential detection methods have the error floor effect. The more the turbulence intensity affects the average BER of the MIMO UWOC system with the increase of the communication link distance, the more obvious is the effect of the turbulence intensity on the average BER of the MIMO UWOC system. Accordingly, the simulation analysis shows that the differential detection method is more suitable for the construction of communication links under long-distance and medium-strong turbulence.



Citation: Wang, T.; Yu, X.; Zhao, B.; Pang, D. Error Characterization of Differential Detection and Non-Differential Detection for MIMO UWOC Systems in Seawater Turbulent Channels. *Photonics* **2023**, *10*, 859. <https://doi.org/10.3390/photonics10080859>

Received: 24 May 2023
Revised: 20 July 2023
Accepted: 22 July 2023
Published: 25 July 2023



Copyright: © 2023 by the authors. Licensee MDPI, Basel, Switzerland. This article is an open access article distributed under the terms and conditions of the Creative Commons Attribution (CC BY) license (<https://creativecommons.org/licenses/by/4.0/>).

Keywords: underwater wireless optical communication; ocean turbulence; differential detection; average bit error rate

1. Introduction

As an important strategic space for sustainable human development, the ocean not only provides sufficient natural gas, oil, and other material energy for people's lives but is also an important strategic high point for military development in the world today [1]. The development of devices, such as marine environmental monitors, underwater high-resolution imaging systems, and autonomous underwater vehicles (AUVs), has increased the need for real-time communication and high-capacity data transmission between underwater end devices [2]. Space laser communication is gradually becoming the main way to solve the problem of underwater high-capacity data transmission because of its strong anti-interference capability [3], high transmission capacity [4], high rate [5], and fast deployment [6]. However, the reasons affecting the development of UWOC are the scattering and absorption of light by seawater and ocean turbulence, where ocean turbulence subject to changes in salinity, temperature, and seawater density is the main factor affecting beam propagation [7]; turbulence especially causes scintillation effects, resulting in the received light energy showing violent jitter, which will seriously degrade the performance of UWOC

systems [8]. To reduce the impact of ocean turbulence on underwater laser communication systems, researchers in various countries have conducted extensive research.

Considering the current similarity between ocean turbulence and atmospheric turbulence, the analysis of the propagation characteristics of ocean turbulence on light waves is mainly based on the classical atmospheric turbulence research results in free optical communication. Ruijie Li et al. [9] took Malaga (M) turbulence channel as an example and analyzed the average error probability with pointing error under atmospheric turbulence channel and also analyzed the BER closure expressions for different modulation techniques under different turbulence conditions. Ansari et al. [10] analyzed the basic functional expressions for pointing error, average BER, and traversal capability based on the Malaga turbulence model to illustrate the impact of atmospheric turbulence intensity and pointing error severity on the performance of communication systems. M. Khalighi et al. [11] artificially reduces the effect of background radiation on terrestrial free-space optical communication systems. They proposed using dual wavelength transmitting data and detecting the data by differential detection mode at the receiving end. In addition, they derived the integral function relationship between the signal-to-noise ratio of differential detection and the average BER. Toselli et al. [12] proposed to reduce the effect of flicker index on the error characteristics of communication systems by using a combination of adaptive optics and aperture averaging.

However, the seawater channel is a complex time-varying channel whose random ups and downs of refractive index are affected by the random changes of seawater temperature and salinity as well as the special characteristics of underwater laser communication wavelengths and detector device performance. In particular, the effect of ocean turbulence on light has a very important role in the design of underwater laser communication systems; thus, the needs of ocean turbulence and high-speed data transmission should be considered comprehensively.

Rahman et al. [13] conducted modeling simulations for multilayer vertical underwater links and analyzed the performance of underwater optical communication systems using ocean turbulence models, such as generalized gamma (GG), exponential GG (EGG), exponentiated Weibull (EW), and gamma-gamma ($\Gamma\Gamma$) as well as derived expressions for the signal-to-noise ratio of the probability density function and cumulative distribution function. Yuqing Fu et al. [14] investigated the effect of aperture averaging on the average BER of DPSK UWOC systems in the case of moderately strong turbulence based on planar and spherical wave transmission models. Meanwhile, Gökçe, Muhsin Caner et al. [15] quantified the improvement of the aperture averaging of Gaussian beams on the average BER of communication systems under weak turbulence conditions. I. Yahya Baykal et al. [16] analyzed the upper bound on the average BER of ppm-owc links operating in ocean turbulence, and simulations verified that the error performance of PPM is better than OOK modulation. Hema, R. et al. [17] proposed a DC-biased optical orthogonal frequency division multiplexing technique with MIMO for underwater wireless optical channels and simulated and analyzed the communication performance in terms of signal-to-noise ratio, channel capacity, and BER under weak turbulence conditions. Jianying Wang et al. [18] analyzed the effect of pointing error and beam spread scenarios on the average BER of MIMO underwater communication systems using the Malaga turbulent channel as an example, although many scholars have analyzed methods to improve the average BER performance in oceanic turbulent channels. However, none of the above literature have analyzed the different detection performance of MIMO UWOC systems under medium-strength turbulence [19]. Medium-strength turbulence is an important component that affects seawater turbulence; thus, it is necessary to analyze the system performance of MIMO UWOC systems from the point of view of practical application and enrichment of theory.

The gamma-gamma model can better simulate the medium-intensity ocean turbulence. This paper analyzes the error characteristics of two MIMO UWOC systems, differential detection, and non-differential detection based on the gamma-gamma turbulence model. The expressions for the average BER calculation of differential detection and non-differential

detection MIMO UWOC under the influence of gamma-gamma turbulence are pushed in the case of completely uncorrelated received signals. Based on the above derived expressions, the effects of turbulence intensity and communication distance on the BER of MIMO UWOC are simulated and analyzed, while the error floor effect of MIMO UWOC detection and reception system is simulated and analyzed, and the average BER performances of differential and non-differential detection in MIMO UWOC are compared.

The novelty of this paper is reflected in the following two aspects:

1. The expressions for calculating the average BER of two MIMO UWOC systems with differential detection and non-differential detection are derived based on the gamma-gamma turbulence model when the two transmitted beams are completely uncorrelated.
2. Simulation demonstrates that the differential detection method has a lower average BER compared with the non-differential detection method from the perspective of ocean turbulence intensity and communication link distance. Additionally, the differential detection method does not have an error flattening effect, while the non-differential detection method has an error flattening effect.

2. UWOC System Modeling

2.1. MIMO UWOC System Transmission Model

The composition of the MIMO-based underwater laser communication system is shown in Figure 1. An example of a differential detection system is shown in Figure 1a. Firstly, the signal-processing board is used to divide the band modulation information into the original signal, S and the inverted signal, \bar{S} , which are then modulated to the lasers with wavelengths, λ_1 and λ_2 , respectively. Affected by the absorption scattering of the water channel, usually underwater optical communication uses emission wavelengths of 450 nm and 532 nm. We designed the transmitting antennas of the two beams to be a few centimeters or closer to each other to ensure that the two beams have the same turbulence impact after passing through the ocean turbulence channel. After passing through the ocean turbulence channel with communication distance, L , to reach the laser communication receiver, let the optical signal reaching the receiver be y_1 and y_2 . First through the optical filter, filter out the background noise and another transmitter light signal after receiving the optical antenna focus to the detector target surface. The photodetector converts the optical signal to the electrical signal, and then the output signal is subtracted and judged to recover the original data transmission information.

The non-differential detection system is shown in Figure 1b. Non-differential detection is different from differential detection in that it does not require the transmit information to be inverted. The two transmit signals are of the same amplitude and same phase. After the modulator is loaded on the laser, which makes the optical signal of the same modulation information that is emitted, the laser emission is completed by the transmitting optical antenna. After the ocean turbulence channel, the receiving optical antenna will focus the spatial light to the detector target surface, and the detector output electrical signal will be superimposed and judged to recover the original data transmission information.

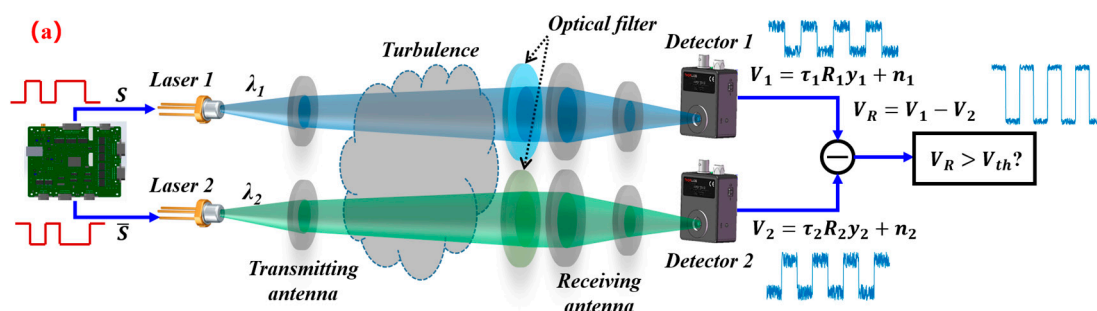


Figure 1. Cont.

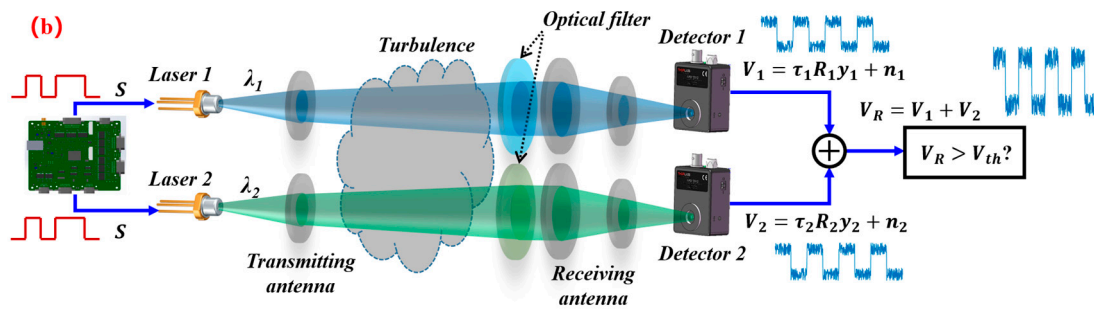


Figure 1. Block diagram of MIMO UWOC system components: (a) block diagram of differential detection system, (b) block diagram of non-differential detection system.

Based on the above theory, it is known that the output signals of the two detectors in the MIMO system are

$$V_1 = \tau_1 R_1 y_1 + n_1 = \tau_1 R_1 S I h_1 + n_1, \tag{1}$$

$$V_2 = \tau_2 R_2 y_2 + n_2 = \tau_2 R_2 \bar{S} I h_2 + n_2, \tag{2}$$

where S is the signal after sending data “1” or “0”. \bar{S} is the signal after sending data inverse when S is 1 and \bar{S} is 0. I is the light intensity when the transmission signal is “1”. n_1 and n_2 are the noise of the two detectors, respectively. The noise satisfies the Gaussian white noise with mean value 0 and variance $N_0/2$. h_1 and h_2 are the random attenuation of the optical signal by ocean turbulence. R_1 and R_2 are the detector photoelectric conversion efficiency. τ_1 and τ_2 are the optical loss of the system. Since the detectors used in the MIMO laser communication system are all the same, the photoelectric conversion efficiency of the detectors can be simplified to $R_1 = R_2 = R$, and the optical loss of the system can be simplified to $\tau_1 = \tau_2 = \tau$.

It follows that the output signal of the differential detection system is

$$V_R = V_1 - V_2 = \tau_1 R_1 S I h_1 - \tau_2 R_2 \bar{S} I h_2 + n_1 - n_2 = \begin{cases} \tau_1 R_1 I h_1 + n_1 - n_2, & S = 1 \\ -\tau_2 R_2 I h_2 + n_1 - n_2, & S = 0' \end{cases} \tag{3}$$

The output signal of the non-differential detection system is

$$V_R = V_1 + V_2 = \tau_1 R_1 S I h_1 + \tau_2 R_2 S I h_2 + n_1 + n_2 = \begin{cases} \tau_1 R_1 I h_1 + \tau_2 R_2 I h_2 + n_1 + n_2, & S = 1 \\ n_1 + n_2, & S = 0 \end{cases} . \tag{4}$$

2.2. UWOC Turbulence Channel Model

According to the literature [20–23], it is known that the gamma-gamma turbulence model can accurately describe the probability density function of the signal light intensity decay under the medium-intensity ocean turbulence effect [24]; thus, the probability density function is expressed as

$$f(h_1) = \frac{2(\alpha_1 \beta_1)}{\Gamma(\alpha_1) \Gamma(\beta_1)} h_1^{\frac{\alpha_1 + \beta_1}{2} - 1} K_{\alpha_1 - \beta_1} \left(2\sqrt{\alpha_1 \beta_1 h_1} \right), \tag{5}$$

$$f(h_2) = \frac{2(\alpha_2 \beta_2)}{\Gamma(\alpha_2) \Gamma(\beta_2)} h_2^{\frac{\alpha_2 + \beta_2}{2} - 1} K_{\alpha_2 - \beta_2} \left(2\sqrt{\alpha_2 \beta_2 h_2} \right), \tag{6}$$

where $K_v(\cdot)$ is a Bessel function of the second kind with order v . $\Gamma(\cdot)$ is expressed as Gamma function. If the optical radiation at the receiving end is a plane wave, α and β in the intensity probability density function are related to ocean conditions [25], which are defined as:

$$\alpha = \left[\exp \left(\frac{0.49\sigma_I^2}{(1 + 1.11\sigma_I^{12/5})^{7/6}} \right) - 1 \right]^{-1}, \tag{7}$$

$$\beta = \left[\exp \left(\frac{0.51\sigma_I^2}{(1 + 0.69\sigma_I^{12/5})^{5/6}} \right) - 1 \right]^{-1}, \tag{8}$$

where σ_I^2 is the Rytov variance of the laser intensity undulation in ocean turbulence. Because of the close distance between the two transmitting antennas, the two light transmissions can be in the same dimensional and weather conditions. Since the value of the turbulence structure constant, C_n^2 , depends on environmental factors, such as also the height and weather conditions, it is known that both beams pass through the same turbulence, $C_{n_1}^2 = C_{n_2}^2 = C_n^2$. For a horizontally propagating optical field in a turbulent medium, the refractive index structure constant, C_n^2 , is a constant value, and the Rytov variance of the plane wave can be expressed as

$$\sigma_I^2 = 1.23C_n^2k^{7/6}L_p^{11/6} \tag{9}$$

where k is the wave vector $k = 2\pi/\lambda$ and λ is the laser carrier wavelength. L_p is the link distance. The design chooses laser emission wavelengths of 450 nm and 532 nm because the distance between the two transmitters and the receiver is the same, and thus, it can be assumed that they pass through the same underwater turbulence channel; we have $\alpha_1 = \alpha_2 = \alpha$ and $\beta_1 = \beta_2 = \beta$. Then the gamma-gamma turbulence model of the MIMO system can be simplified as

$$f(h_1) = \frac{2(\alpha\beta)^{\frac{\alpha+\beta}{2}}}{\Gamma(\alpha)\Gamma(\beta)} h_1^{\frac{\alpha+\beta}{2}-1} K_{\alpha-\beta} \left(2\sqrt{\alpha\beta}h_1 \right), \tag{10}$$

$$f(h_2) = \frac{2(\alpha\beta)^{\frac{\alpha+\beta}{2}}}{\Gamma(\alpha)\Gamma(\beta)} h_2^{\frac{\alpha+\beta}{2}-1} K_{\alpha-\beta} \left(2\sqrt{\alpha\beta}h_2 \right). \tag{11}$$

3. MIMO System Error Characterization

The UWOC system is designed using intensity modulation/direct detection (IM/DD) without considering external factors, such as receiver alignment problems in the communication system, background light in the channel, and other interference between devices. Assuming that the communication system is affected only by the fading and additive Gaussian white noise under the transmission path of the turbulent channel, the instantaneous BER equation can be expressed as

$$P_e = P(0)P(e/0) + P(1)P(e/1), \tag{12}$$

where $P(0)$ and $P(1)$ are the probabilities of sending data 1 and 0 with a mean value of 0.5. $P(e/0)$ is the probability that a “0” pulse is incorrectly judged as a “1”. $P(e/1)$ is the probability that a “1” pulse is incorrectly judged as a “0”.

3.1. Derivation of the Average BER at Differential Detection

If the sent data amplitude satisfies the normal distribution, then the probability of sending a “1” code satisfies $N[(\tau R I h_1), N_0]$, and N_0 is the variance. The probability of sending a “0” code satisfies $N[(\tau R I h_2), N_0]$ so that the instantaneous error rate of a wrong decision is

$$P(e/0) = \int_{v_{th}}^{\infty} \frac{1}{\sqrt{2\pi N_0}} \exp \left[-\frac{(x + \tau R I h_2)^2}{2N_0} \right] dx = \frac{1}{2} \operatorname{erfc} \left(\frac{v_{th} + \tau R I h_2}{\sqrt{2N_0}} \right), \tag{13}$$

$$P(e/1) = \int_{-\infty}^{v_{th}} \frac{1}{\sqrt{2\pi N_0}} \exp\left[-\frac{(x - \tau R I h_1)^2}{2N_0}\right] dx = \frac{1}{2} \operatorname{erfc}\left(\frac{\tau R I h_1 - v_{th}}{\sqrt{2N_0}}\right), \tag{14}$$

where $\operatorname{erfc}(x) = \frac{2}{\sqrt{\pi}} \int_x^\infty e^{-\eta^2} d\eta$ is the complementary error function. Then, the average BER of the MIMO system can be expressed as

$$\langle P_e \rangle = \int_0^\infty \int_0^\infty f(h_1, h_2) P_e dh_1 dh_2, \tag{15}$$

where $f(h_1, h_2)$ is the joint probability density of h_1 and h_2 . For two signals that are completely uncorrelated, then, h_1 and h_2 obey the same gamma-gamma distribution, so $h_1 = h_2 = h$. When the judgment threshold is an over-zero judgment, the instantaneous BER at which an erroneous judgment occurs can be simplified as

$$P(e/0) = P(e/1) = \frac{1}{2} \operatorname{erfc}\left(\frac{\tau R I h}{\sqrt{2N_0}}\right). \tag{16}$$

Then, the average BER of differential detection is simplified as

$$\langle P_e \rangle = \int_0^\infty f(h) P_e dh. \tag{17}$$

Bringing Equations (10)–(12) and (16) into Equation (17) yields

$$\langle P_e \rangle = \frac{(\alpha\beta)^{\frac{\alpha+\beta}{2}}}{\Gamma(\alpha)\Gamma(\beta)} \int_0^\infty h^{\frac{\alpha+\beta}{2}-1} K_{\alpha-\beta}(2\sqrt{\alpha\beta}h) \operatorname{erfc}\left(\frac{\tau R I h}{\sqrt{2N_0}}\right) dh, \tag{18}$$

Based on the performance of the Meijer G function $K_v(\cdot) = \frac{1}{2} G_{0,2}^{2,0} \left[\frac{x^2}{4} \middle| v/2, -v/2 \right]$, $\operatorname{erfc}(\sqrt{x}) = \frac{1}{\sqrt{\pi}} G_{1,2}^{2,0} \left[x \middle| 1, 1/2 \right]$ and Equation (21) in the literature [26], Equation (18) can be reduced (see Appendix A for details of the reduction process).

$$\langle P_e \rangle = \frac{2^{\alpha+\beta-3}}{\pi^{3/2}\Gamma(\alpha)\Gamma(\beta)} G_{5,2}^{2,4} \left(\frac{8\tau^2}{\alpha^2\beta^2} \gamma_0 \left[\frac{1-\alpha}{2}, \frac{2-\alpha}{2}, \frac{1-\beta}{2}, \frac{2-\beta}{2}, 1 \right] \right), \tag{19}$$

3.2. Derivation of Average BER for Non-Differential Detection

If the sent data amplitude satisfies the normal distribution, then the probability of sending a “1” code satisfies $N[(\tau R I h_1 + \tau R I h_2), N_0]$, and N_0 is the variance so that the instantaneous error rate of a wrong decision is:

$$P(e/0) = \int_{v_{th}}^\infty \frac{1}{\sqrt{2\pi N_0}} \exp\left[-\frac{x^2}{2N_0}\right] dx = \frac{1}{2} \operatorname{erfc}\left(\frac{v_{th}}{\sqrt{2N_0}}\right), \tag{20}$$

$$\begin{aligned} P(e/1) &= \int_{-\infty}^{v_{th}} \frac{1}{\sqrt{2\pi N_0}} \exp\left[-\frac{(x - \tau R I h_1 - \tau R I h_2)^2}{2N_0}\right] dx \\ &= \frac{1}{2} \operatorname{erfc}\left(\frac{\tau R I h_1 + \tau R I h_2 - v_{th}}{\sqrt{2N_0}}\right) \end{aligned}, \tag{21}$$

When the judgment threshold uses over-zero judgment, the instantaneous BER at which an erroneous judgment occurs can be simplified as

$$P(e/0) = \frac{1}{2} \operatorname{erfc} \left(\frac{0}{\sqrt{2N_0}} \right) = \frac{1}{2}, \tag{22}$$

$$P(e/1) = \frac{1}{2} \operatorname{erfc} \left(\frac{\tau R I h_1 + \tau R I h_2}{\sqrt{2N_0}} \right), \tag{23}$$

Because $h_1 = h_2 = h$, then the instantaneous BER at which an error judgment occurs $P(e/1)$ can be simplified as

$$P(e/1) = \frac{1}{2} \operatorname{erfc} \left(\frac{2\tau R I h - v_{th}}{\sqrt{2N_0}} \right), \tag{24}$$

Then, the average BER of non-differential detection is simplified as

$$\langle P_e \rangle = \int_0^\infty f(h) P(0) P(e/0) + f(h) P(1) P(e/1) dh, \tag{25}$$

Based on the performance of the Meijer G function, the average BER formula for non-differential detection can be obtained by bringing Equations (10), (22) and (24) into Equation (25) (see Appendix B for details of the derivation process).

$$\begin{aligned} \langle P_e \rangle &= \frac{\alpha\beta}{4\Gamma(\alpha)\Gamma(\beta)(1-\alpha)(1-\beta)} \\ &+ \frac{2^{\alpha+\beta-4}}{\pi^{3/2}\Gamma(\alpha)\Gamma(\beta)} G_{5,2}^{2,4} \left(\frac{8\tau^2}{\alpha^2\beta^2} \gamma_0 \left| \begin{matrix} \frac{1-\alpha}{2}, \frac{2-\alpha}{2}, \frac{1-\beta}{2}, \frac{2-\beta}{2}, 1 \\ 0, \frac{1}{2} \end{matrix} \right. \right). \end{aligned} \tag{26}$$

4. Numerical Simulation of MIMO UWOC System

The BER performance of the MIMO UWOC system is simulated and analyzed, and the parameters used in the simulation process are shown in Table 1. The distance between the two beams is set to be similar in the simulation process so their ocean turbulence attenuation coefficients obey the gamma-gamma function with the same parameters.

Table 1. MIMO UWOC Simulation Parameters.

Parameter	Value	Unit
Wavelength, λ	450, 532	nm
Turbulence structure constant, C_n^2	8.5×10^{-15} , 1.5×10^{-14} , 5.0×10^{-14}	$m^{-2/3}$
Photoelectric conversion efficiency, R	1	A/W
Link distance, L	1000, 3000	m
Optical loss rate, τ	0.8	%
Signal to ratio, γ_0	0–100	dB

4.1. Analysis of Ocean Turbulence Intensity on the Average BER of MIMO UWOC Systems

To analyze the error characteristics of marine turbulence on the MIMO communication system, the average BER versus SNR curves of MIMO are simulated for weak, medium, and strong turbulence, $C_n^2 = 8.5 \times 10^{-15}$, 1.5×10^{-14} , 5.0×10^{-14} , at a link distance of 1 km. The simulation results are shown in Figure 2.

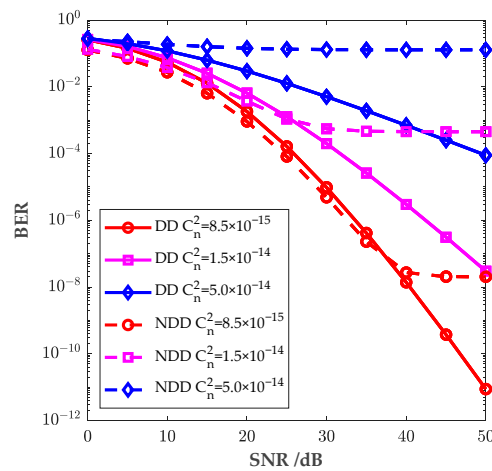


Figure 2. Average BER of DD and NDD under different turbulence intensity conditions.

According to the simulation results, the average BER of DD and NDD MIMO communication systems increases gradually with the increase of turbulence intensity at the same SNR. For the same average, $BER = 2.28 \times 10^{-7}$, the required SNR of DD under weak turbulence, $C_n^2 = 8.5 \times 10^{-15}$, is 35 dB less than that under medium turbulence $C_n^2 = 1.5 \times 10^{-14}$ of 45 dB.

In the case of $C_n^2 = 8.5 \times 10^{-15}$, the average BER of the MIMO system with NDD is better than that of differential detection when the SNR is less than 33 dB. When the signal-to-noise ratio is greater than 33 dB, the average BER of DD is better than that of NDD.

4.2. Analysis of Link Distance on the Average BER of MIMO UWOC Systems

The turbulence structure constant is set to $C_n^2 = 1.5 \times 10^{-14} \text{ m}^{-2/3}$, and the average BER of differential detection and non-differential detection MIMO systems with link distances of $L = 1 \text{ km}$ and 2 km are analyzed, respectively. The simulation results are shown in Figure 3, the longer the link distance, the worse the average BER of the MIMO system. The reason for the above phenomenon is that when the transmission distance increases, the probability of detecting the deep fading of the received signal light intensity increases, and the fading of the light intensity makes the signal light smaller than the background noise at the receiver side, which makes the judgment of the data incorrect so the link distance has a greater impact on the average BER of the DD MIMO system.

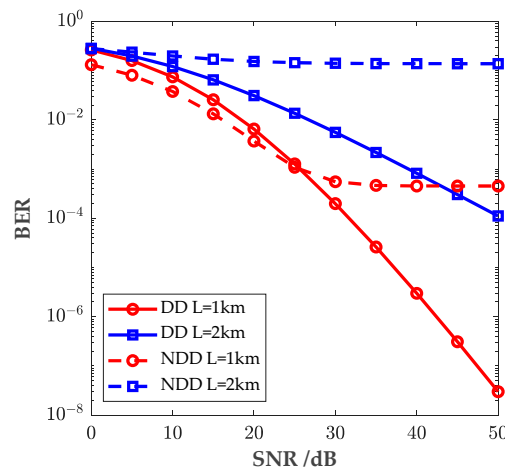


Figure 3. Average BER of DD and NDD under different communication distance conditions.

4.3. Analysis of Error Floor Effect of MIMO UWOC System

The error-flooring effect is that when the signal-to-noise ratio is raised to a certain value, the BER is maintained at a fixed level without decreasing. In order to analyze whether the differential detection system can overcome the error floor effect, the average BER curve of DD with the signal-to-noise ratio in the 0–120 dB range is simulated, and the simulation results are shown in Figure 4.

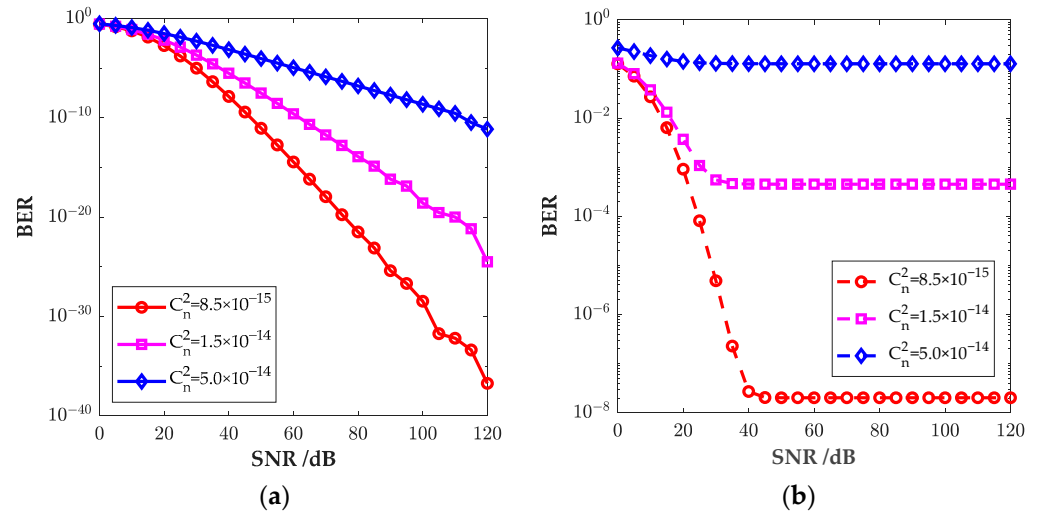


Figure 4. Analysis curve of error floor effect of MIMO communication system: (a) differential detection (b) non-differential detection.

The simulation results show that the average BER of the DD MIMO communication system keeps decreasing with the increase of SNR; thus, it is concluded that there is no error-flattening effect in the differential detection MIMO communication system. In the weak turbulence case of $C_n^2 = 8.5 \times 10^{-15}$, the average BER of the non-differential detection system does not decrease with the increase of SNR after the SNR increases to 40 dB.

5. Conclusions

In this paper, the error characteristics of the MIMO underwater wireless optical communication system are analyzed, and the average BER expressions for the two cases of differential detection and non-differential detection are derived based on the gamma-gamma turbulence model. The average BER performance of the MIMO UWOC system is simulated and analyzed in terms of both ocean turbulence intensity and communication distance. The simulation results show that when the signal-to-noise ratio increases to 40 dB, the non-differential detection system shows the error floor effect, while the differential detection system does not have the error floor effect. The longer the communication link distance, the more obvious the effect of ocean turbulence on the average BER of the MIMO system, and the average BER of the differential detection is better than that of the non-differential detection system. Therefore, the differential detection provides theoretical support for the establishment of long-range UWOC links under moderately strong turbulence.

Author Contributions: T.W. contributed to the conception of the study and writing of the manuscript; X.Y. and D.P. made important contributions to the analysis of the differential detection simulations; B.Z. helped with the translation analysis of the paper and the related literature search. All authors have read and agreed to the published version of the manuscript.

Funding: Equipment pre-research application innovation project (62602010125); National Key R&D Program Project “Intersatellite Laser Communication Measurement Integrated System Technology” (2022YFB3902500); National Key R&D Program Project “Verification of High Temperature Superconducting Single Photon Detector Laser Communication Application” (2021YFA0718804), National Natural Science Foundation of China (U2141231).

Institutional Review Board Statement: The study did not require ethical approval.

Informed Consent Statement: The study did not involve humans.

Data Availability Statement: Not applicable.

Conflicts of Interest: No conflict of interest exist in the submission of this manuscript, and the manuscript is approved by all authors for publication. I would like to declare on behalf of my co-authors that the work described was original research that has not been published previously and is not under consideration for publication elsewhere in whole or in part. All authors listed have approved the manuscript that is enclosed.

Appendix A

The derivation process of the average error rate formula for differential detection

$$\begin{aligned} \langle P_e \rangle &= \frac{(\alpha\beta)^{\frac{\alpha+\beta}{2}}}{\Gamma(\alpha)\Gamma(\beta)} \int_0^\infty h^{\frac{\alpha+\beta}{2}-1} K_{\alpha-\beta}(2\sqrt{\alpha\beta h}) \operatorname{erfc}\left(\frac{\tau R I h}{\sqrt{2N_0}}\right) dh \\ &= \frac{(\alpha\beta)^{\frac{\alpha+\beta}{2}}}{\Gamma(\alpha)\Gamma(\beta)} \int_0^\infty h^{\frac{\alpha+\beta}{2}-1} \frac{1}{2} G_{0,2}^{2,0} \left[\alpha\beta h \left| \begin{matrix} 0 \\ \frac{\alpha-\beta}{2}, \frac{\beta-\alpha}{2} \end{matrix} \right. \right] \cdot \frac{1}{\sqrt{\pi}} G_{1,2}^{2,0} \left[\frac{\tau^2 R^2 I^2 h^2}{2N_0} \left| \begin{matrix} 1 \\ 0, \frac{1}{2} \end{matrix} \right. \right] dh \end{aligned}$$

Organized:

$$\langle P_e \rangle = \frac{(\alpha\beta)^{\frac{\alpha+\beta}{2}}}{2\sqrt{\pi}\Gamma(\alpha)\Gamma(\beta)} \int_0^\infty h^{\frac{\alpha+\beta}{2}-1} G_{0,2}^{2,0} \left[\alpha\beta h \left| \begin{matrix} 0 \\ \frac{\alpha-\beta}{2}, \frac{\beta-\alpha}{2} \end{matrix} \right. \right] \cdot G_{1,2}^{2,0} \left[\frac{\tau^2 R^2 I^2 h^2}{2N_0} \left| \begin{matrix} 1 \\ 0, \frac{1}{2} \end{matrix} \right. \right] dh$$

According to the Meijer G integral properties in the references:

$$\begin{aligned} &\int_0^\infty x^{\alpha-1} G_{u,v}^{s,t} \left(ox \left| \begin{matrix} (o_u) \\ (d_v) \end{matrix} \right. \right) G_{p,q}^{m,n} \left(\omega x^{\ell/k} \left| \begin{matrix} (a_p) \\ (b_q) \end{matrix} \right. \right) dx \\ &= \frac{k^u}{(2\pi)^{b^*(\ell-1)+o^*(k-1)}} G_{kp+\ell v, kq+\ell u}^{km+\ell t, kn+\ell s} \left(\frac{\omega^k k^{k(p-q)}}{o^\ell \ell^{\ell(u-v)}} \left| \begin{matrix} \Delta(k, a_1), \dots, \Delta(k, a_n), \Delta(\ell, 1-\alpha-d_v), \Delta(k, a_{n+1}), \dots, \Delta(k, a_p) \\ \Delta(k, b_1), \dots, \Delta(k, b_n), \Delta(\ell, 1-\alpha-o_1), \Delta(k, b_{m+1}), \dots, \Delta(k, b_q) \end{matrix} \right. \right) \end{aligned}$$

where $\Delta(k, a) = \frac{a}{k}, \frac{a+1}{k}, \dots, \frac{a+k-1}{k}$, $b^* = s + t - (u + v)/2$, $c^* = m + n - (p + q)/2$
 Substitution can obtain:

$$\begin{aligned} \langle P_e \rangle &= \frac{(\alpha\beta)^{\frac{\alpha+\beta}{2}}}{2\sqrt{\pi}\Gamma(\alpha)\Gamma(\beta)} \cdot \frac{2^{\alpha+\beta-1}}{2\pi} (\alpha\beta)^{-\frac{\alpha+\beta}{2}} \\ &\cdot G_{k+2l, 2k}^{2k, 2l} \left[\frac{\tau^2 R^2 I^2 k^{-k}}{2N_0(\alpha\beta)^{\ell|\ell|}} \left| \begin{matrix} \Delta(k, 1), \Delta(l, 1-\alpha), \Delta(l, 1-\beta) \\ \Delta(k, 0), \Delta\left(k, \frac{1}{2}\right) \end{matrix} \right. \right] \\ &= \frac{2^{\alpha+\beta-3}}{\pi^{3/2}\Gamma(\alpha)\Gamma(\beta)} G_{5,2}^{2,4} \left(\frac{\tau^2 8}{\alpha^2 \beta^2} \gamma_0 \left| \begin{matrix} \frac{1-\alpha}{2}, \frac{2-\alpha}{2}, \frac{1-\beta}{2}, \frac{2-\beta}{2} \\ 0, \frac{1}{2} \end{matrix} \right. \right) \end{aligned}$$

Appendix B

The derivation process of non-differential detection:

$$\begin{aligned} \langle P_e \rangle &= \int_0^\infty f(h)P(0)P(e/0) + f(h)P(1)P(e/1)dh \\ &= \int_0^\infty f(h)P(0)P(e/0)dh + \int_0^\infty f(h)P(1)P(e/1)dh \\ &= \frac{2(\alpha\beta)}{4\Gamma(\alpha)\Gamma(\beta)} \int_0^\infty h^{\frac{\alpha+\beta}{2}-1} K_{\alpha-\beta}(2\sqrt{\alpha\beta h_2}) dh \\ &+ \frac{(\alpha\beta)^{\frac{\alpha+\beta}{2}}}{2\Gamma(\alpha)\Gamma(\beta)} \int_0^\infty h^{\frac{\alpha+\beta}{2}-1} K_{\alpha-\beta}(2\sqrt{\alpha\beta h}) \operatorname{erfc}\left(\frac{\tau R I h}{\sqrt{2N_0}}\right) dh \\ &= \langle P_{e1} \rangle + \langle P_{e2} \rangle \end{aligned}$$

$$\begin{aligned}
 \langle P_{e1} \rangle &= \frac{(\alpha\beta)^{\frac{\alpha+\beta}{2}}}{2\Gamma(\alpha)\Gamma(\beta)} \int_0^\infty h^{\frac{\alpha+\beta}{2}-1} K_{\alpha-\beta}(2\sqrt{\alpha\beta h}) dh \\
 &= \frac{(\alpha\beta)^{\frac{\alpha+\beta}{2}}}{2\Gamma(\alpha)\Gamma(\beta)} \int_0^\infty h^{\frac{\alpha+\beta}{2}-1} \frac{1}{2} G_{0,2}^{2,0} \left[\alpha\beta h \left| \begin{matrix} 0 \\ \frac{\alpha-\beta}{2}, \frac{\beta-\alpha}{2} \end{matrix} \right. \right] dh \\
 &= \frac{(\alpha\beta)^{\frac{\alpha+\beta}{2}}}{4\Gamma(\alpha)\Gamma(\beta)} \frac{\prod_{k=1}^2 \Gamma\left(\frac{\alpha+\beta}{2} + b_k\right)}{\prod_{k=1}^2 \Gamma\left(1 - \frac{\alpha+\beta}{2} - b_k\right)} (\alpha\beta)^{-\frac{\alpha+\beta}{2}} \\
 &= \frac{\alpha\beta}{4\Gamma(\alpha)\Gamma(\beta)(1-\alpha)(1-\beta)} \\
 \langle P_{e2} \rangle &= \frac{(\alpha\beta)^{\frac{\alpha+\beta}{2}}}{2\Gamma(\alpha)\Gamma(\beta)} \int_0^\infty h^{\frac{\alpha+\beta}{2}-1} K_{\alpha-\beta}(2\sqrt{\alpha\beta h}) \operatorname{erfc}\left(\frac{\tau R I h}{\sqrt{2N_0}}\right) dh \\
 &= \frac{(\alpha\beta)^{\frac{\alpha+\beta}{2}}}{2\Gamma(\alpha)\Gamma(\beta)} \int_0^\infty h^{\frac{\alpha+\beta}{2}-1} \frac{1}{2} G_{0,2}^{2,0} \left[\alpha\beta h \left| \begin{matrix} 0 \\ \frac{\alpha-\beta}{2}, \frac{\beta-\alpha}{2} \end{matrix} \right. \right] \cdot \frac{1}{\sqrt{\pi}} G_{1,2}^{2,0} \left[\frac{\tau^2 R^2 I^2 h^2}{2N_0} \left| \begin{matrix} 1 \\ 0, \frac{1}{2} \end{matrix} \right. \right] dh \\
 &= \frac{2^{\alpha+\beta-4}}{\pi^{3/2}\Gamma(\alpha)\Gamma(\beta)} G_{5,2}^{2,4} \left(\frac{8\tau^2}{\alpha^2\beta^2} \gamma_0 \left| \begin{matrix} \frac{1-\alpha}{2}, \frac{2-\alpha}{2}, \frac{1-\beta}{2}, \frac{2-\beta}{2} \\ 0, \frac{1}{2} \end{matrix} \right. , 1 \right)
 \end{aligned}$$

Therefore, it can be concluded that

$$\begin{aligned}
 \langle P_e \rangle &= \langle P_{e1} \rangle + \langle P_{e2} \rangle \\
 &= \frac{\alpha\beta}{4\Gamma(\alpha)\Gamma(\beta)(1-\alpha)(1-\beta)} \\
 &\quad + \frac{2^{\alpha+\beta-4}}{\pi^{3/2}\Gamma(\alpha)\Gamma(\beta)} G_{5,2}^{2,4} \left(\frac{8\tau^2}{\alpha^2\beta^2} \gamma_0 \left| \begin{matrix} \frac{1-\alpha}{2}, \frac{2-\alpha}{2}, \frac{1-\beta}{2}, \frac{2-\beta}{2} \\ 0, \frac{1}{2} \end{matrix} \right. , 1 \right)
 \end{aligned}$$

References

1. Ali, M.F.; Jayakody, D.N.K.; Li, Y. Recent trends in underwater visible light communication (uvlc) systems. *IEEE Access* **2022**, *10*, 22169–22225. [\[CrossRef\]](#)
2. Ghazy, A.S.; Hranilovic, S.; Khalighi, M. Angular mimo for underwater wireless optical communications: Link modeling and tracking. *IEEE J. Ocean. Eng.* **2021**, *46*, 1391–1407. [\[CrossRef\]](#)
3. Salama, W.M.; Aly, M.H.; Amer, E.S. Underwater optical wireless communication system: Deep learning cnn with noma-based performance analysis. *Opt. Quantum Electron.* **2023**, *55*, 436. [\[CrossRef\]](#)
4. El-Mottaleb, S.A.A.; Singh, M.; Atieh, A.; Aly, M.H. Ocdma transmission-based underwater wireless optical communication system: Performance analysis. *Opt. Quantum Electron.* **2023**, *55*, 465. [\[CrossRef\]](#)
5. Guo, J.; Xiao, J.; Chen, J.; Shan, X.; Kong, D.; Wu, Y.; Ai, Y. Performance analysis of ldpc-coded ofdm in underwater wireless optical communications. *Photonics* **2023**, *10*, 330. [\[CrossRef\]](#)
6. Lin, Z.; Xu, G.; Zhang, Q.; Song, Z. Scintillation index for spherical wave propagation in anisotropic weak oceanic turbulence with aperture averaging under the effect of inner scale and outer scale. *Photonics* **2022**, *9*, 458. [\[CrossRef\]](#)
7. Weng, Y.; Guo, Y.; Alkhazragi, O.; Ng, T.K.; Guo, J.; Ooi, B.S. Impact of turbulent-flow-induced scintillation on deep-ocean wireless optical communication. *J. Light. Technol.* **2019**, *37*, 5083–5090. [\[CrossRef\]](#)
8. Liu, J.; Dong, Y. On Capacity of Underwater Optical Wireless Links under Weak Oceanic Turbulence. In Proceedings of the OCEANS 2016—Shanghai, Shanghai, China, 10–13 April 2016; 2016.
9. Li, R.; Luo, Y.; Dang, A. Unified expressions of ase_p over Málaga (m) turbulence channel. *Opt. Commun.* **2018**, *423*, 74–80. [\[CrossRef\]](#)
10. Ansari, I.S.; Yilmaz, F.; Alouini, M. Performance analysis of free-space optical links over Málaga (M) turbulence channels with pointing errors. *IEEE Trans. Wirel. Commun.* **2016**, *15*, 91–102. [\[CrossRef\]](#)
11. Khalighi, M.; Xu, F.; Jaafar, Y.; Bourennane, S. Double-laser differential signaling for reducing the effect of background radiation in free-space optical systems. *J. Opt. Commun. Netw.* **2011**, *3*, 145–154. [\[CrossRef\]](#)
12. Toselli, I.; Gladysz, S. Improving system performance by using adaptive optics and aperture averaging for laser communications in oceanic turbulence. *Opt. Express* **2020**, *28*, 17347–17361. [\[CrossRef\]](#)
13. Rahman, Z.; Tailor, N.V.; Zafaruddin, S.M.; Chaubey, V.K. Unified performance assessment of optical wireless communication over multi-layer underwater channels. *IEEE Photonics J.* **2022**, *14*, 7349114. [\[CrossRef\]](#)
14. Fu, Y.; Huang, C.; Du, Y. Effect of aperture averaging on mean bit error rate for uwoc system over moderate to strong oceanic turbulence. *Opt. Commun.* **2019**, *451*, 6–12. [\[CrossRef\]](#)
15. Gökçe, M.C.; Baykal, Y. Aperture averaging and ber for gaussian beam in underwater oceanic turbulence. *Opt. Commun.* **2018**, *410*, 830–835. [\[CrossRef\]](#)

16. Baykal, Y.; Ata, Y.; Gökçe, M.C. Underwater turbulence, its effects on optical wireless communication and imaging: A review. *Opt. Laser Technol.* **2022**, *156*, 108624. [[CrossRef](#)]
17. Hema, R.; Sudha, S.; Aarthi, K. Performance studies of mimo based dco-ofdm in underwater wireless optical communication systems. *J. Mar. Sci. Technol.* **2021**, *26*, 97–107. [[CrossRef](#)]
18. Wang, J.; Yin, H.; Ji, X.; Liang, Y. Performance analysis of mimo-mqam system with pointing errors and beam spreading in underwater Málaga turbulence channel. *J. Mar. Sci. Eng.* **2023**, *11*, 633. [[CrossRef](#)]
19. Zhang, J.; Kou, L.; Yang, Y.; He, F.; Duan, Z. Monte-carlo-based optical wireless underwater channel modeling with oceanic turbulence. *Opt. Commun.* **2020**, *475*, 126214. [[CrossRef](#)]
20. Kumar, L.B.; Krishnan, P. Multi-hop convergent fso-uwoc system to establish a reliable communication link between the islands. *Opt. Commun.* **2020**, *474*, 126107. [[CrossRef](#)]
21. Fu, Y.; Duan, Q.; Huang, C.; Du, Y.; Zhou, L. Average ber performance of rectangular qam-uwoc over strong oceanic turbulence channels with pointing error. *Opt. Commun.* **2020**, *476*, 126362. [[CrossRef](#)]
22. Yi, X.; Li, Z.; Liu, Z. Underwater optical communication performance for laser beam propagation through weak oceanic turbulence. *Appl. Opt.* **2015**, *54*, 1273–1278. [[CrossRef](#)]
23. Zhang, J.; Gao, G.; Li, J.; Ma, Z.; Guo, Y. Experimental demonstration and simulation of bandwidth-limited underwater wireless optical communication with mlse. *Photonics* **2022**, *9*, 182. [[CrossRef](#)]
24. Srivastava, V.; Mandloi, A. Performance investigation of wavelength diversity based bpsk-sim fso system under gamma-gamma fading and misalignment error. *Opt. Quantum Electron.* **2021**, *53*, 649. [[CrossRef](#)]
25. Levidala, B.K.; Ramavath, P.N.; Krishnan, P. Performance enhancement using multiple input multiple output in dual-hop convergent underwater wireless optical communication-free-space optical communication system under strong turbulence with pointing errors. *Opt. Eng.* **2021**, *60*, 106106. [[CrossRef](#)]
26. Adamchik, V.; Marichev, O. *The Algorithm for Calculating Integrals of Hypergeometric Type Functions and Its Realization in Reduce System*; ACM: Singapore, 1990.

Disclaimer/Publisher’s Note: The statements, opinions and data contained in all publications are solely those of the individual author(s) and contributor(s) and not of MDPI and/or the editor(s). MDPI and/or the editor(s) disclaim responsibility for any injury to people or property resulting from any ideas, methods, instructions or products referred to in the content.